ORGANIC PROCESS RESEARCH & DEVELOPMENT
OPR&D

Full Paper

Development of a Practical Synthesis of ERK Inhibitor GDC-0994

Xin Linghu, Nicholas Wong, Hans Iding, Vera Jost, Haiming Zhang, Stefan G. Koenig, C. Gregory Sowell, and Francis Gosselin

Org. Process Res. Dev., **Just Accepted Manuscript** • DOI: 10.1021/acs.oprd.7b00006 • Publication Date (Web): 23 Feb 2017

ACS Publications

Organic Process Research & Development is published by the American Chemical Society. 1155 Sixteenth Street N.W., Washington, DC 20036

Development of a Practical Synthesis of ERK Inhibitor GDC-0994

Xin Linghu,*,[†] Nicholas Wong,[†] Hans Iding,[‡] Vera Jost,[‡] Haiming Zhang,[†] Stefan G. Koenig,[†] C. Gregory Sowell,[†] and Francis Gosselin[†]

[†]Small Molecule Process Chemistry, Genentech, Inc., 1 DNA Way, South San Francisco, California 94080, United States
[‡]Process Research, F. Hoffmann-La Roche AG, Grenzacherstrasse 124, CH-4070 Basel, Switzerland

Corresponding Author
*E-mail: linghux@gene.com.

For Table of Contents Only

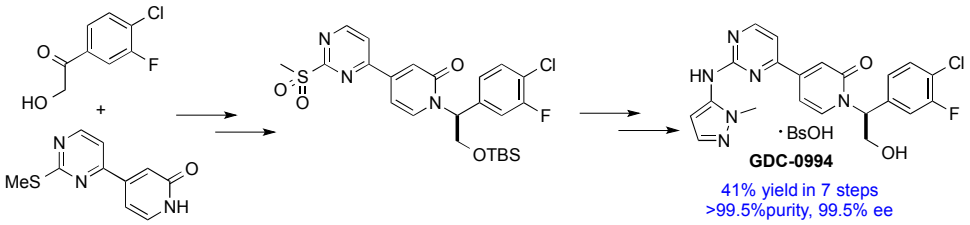

ABSTRACT

The process development of a synthetic route to manufacture ERK inhibitor GDC-0994 on multi-kilogram scale is reported herein. The API was prepared as the corresponding benzenesulfonate salt in 7 steps and 41% overall yield. The synthetic route features a biocatalytic asymmetric ketone reduction, a regioselective pyridone S_N2 reaction and a safe and scalable tungstate-catalyzed sulfide oxidation. The end-game process involves a telescoped S_NAr / desilylation / benzenesulfonate salt formation sequence. Finally, development of the API crystallization allowed purging of process-related impurities, obtaining >99.5A% HPLC and >99% ee of the target molecule.

Keywords: biocatalytic asymmetric ketone reduction; regioselective S_N2 of pyridone; tungstate-catalyzed oxidation; S_NAr displacement of sulfone; one-pot desilylation / salt formation.

1. INTRODUCTION

The extracellular-signal-regulated kinases (ERK1 and ERK2) represent an essential node within the Ras-Raf-MEK-ERK signaling cascade that controls a number of fundamental cellular processes including cell survival, proliferation, motility, and differentiation.[1] Once activated, ERK1/2 kinases phosphorylate several downstream targets involved in cytoskeletal changes and transcriptional activation.[2-5] Furthermore, mutations of upstream genes (Ras and BRAF) that involve a pathway reactivation through ERK1/2 have been identified in many human tumors.[6-8] These observations have promoted the development of several small molecule inhibitors targeting ERK1/2 kinases.[9-15] GDC-0994 (Figure 1) was discovered as a potent, selective, and efficacious inhibitor of ERK1/2 kinases.[16,17] We describe herein an efficient multi-kilogram scale asymmetric synthesis of GDC-0994 to support the preclinical and clinical studies.

Figure 1. Structure of ERK inhibitor GDC-0994

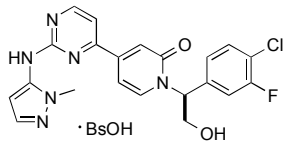

GDC-0994

2. DISCUSSION AND RESULTS

Discovery Synthesis. The initial discovery synthesis of GDC-0994 free-base is outlined in Scheme 1. This route comprises 7 synthetic steps and the target molecule was produced in 12% overall yield. Chiral diol **2** was generated via an osmium-catalyzed asymmetric Sharpless dihydroxylation of styrene **1**. After selective mono-protection as a TBS-ether and mesylation of diol **2**, the S_N2 reaction between pyridone **5**[18] and secondary methanesulfonate **4** was able to produce sulfide **6**. Sulfone **7** was obtained via an oxidation of **6** with *m*-CPBA. Finally, GDC-0994 free-base **10** was synthesized through a

sequence of S_NAr displacement of sulfone **7** with commercially available aminopyrazole **8**, followed by desilylation. While this route enabled the production of hundred-gram quantities of GDC-0994 free-base for preclinical studies, the chemistry suffered from low yields and modest selectivity in several steps. In addition, tedious purification procedures such as distillation and flash chromatography were required due to fairly complex reaction profiles. Issues revolving around process efficiency, reaction safety and robustness deterred the chemistry from being used on multi-kilogram scale.

Scheme 1. Discovery synthetic route to GDC-0994 free-base

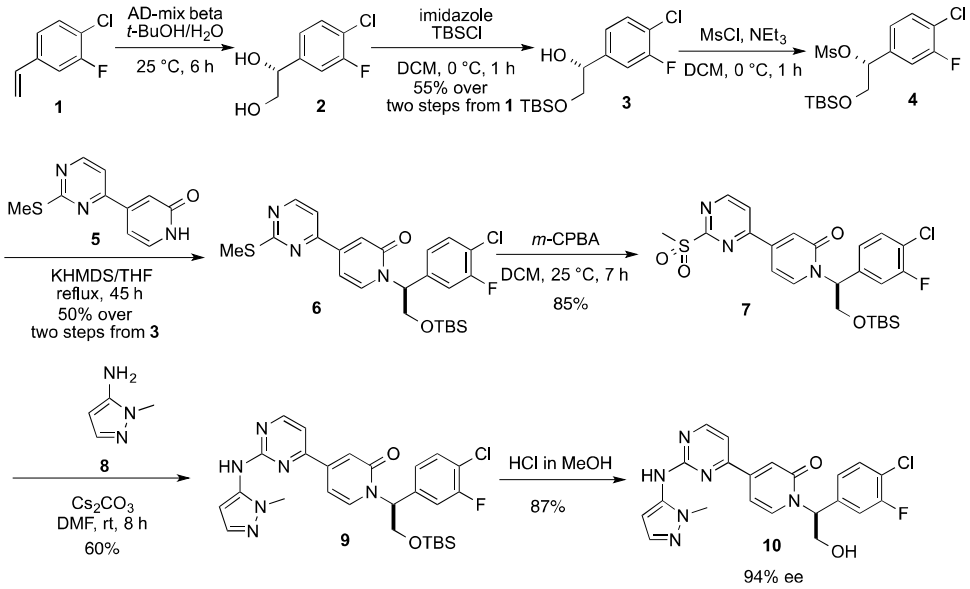

Efficient Asymmetric Synthesis of Chiral Diol. In the original route, chiral diol **2** was synthesized from styrene **1** through a Sharpless asymmetric dihydroxylation. The chiral diol was obtained in 94% ee, a result acceptable for early stage research, but not for our clinical quality requirements. While chiral purity could not be further upgraded in the downstream chemistry and isolations, a selective crystallization of racemic GDC-0994 free-base allowed for the desired (*S*)-enantiomer to reach 98.9% ee in the mother liquor (Scheme 2). Although this process could upgrade chiral purity to an acceptable level, the

inherent mass loss of the desired product rendered it less efficient. In addition to the optical purity issue, tedious purifications were involved in this route, which were considered non-optimal and preferably removed from the process.

Scheme 2. Chiral purity upgrade of GDC-0994 free-base via a selective crystallization of API racemate

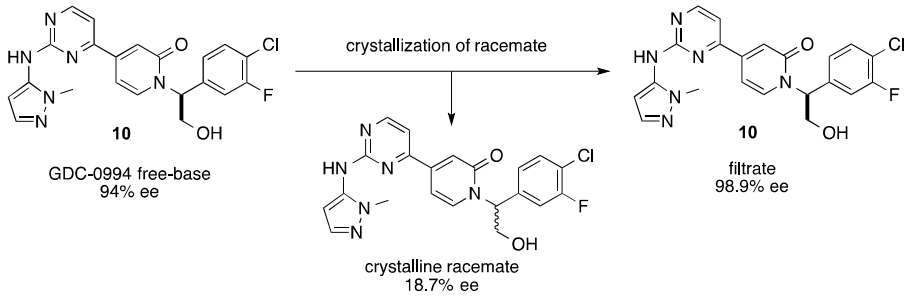

Ketoreductase (KRED)-mediated biotransformations have proven exceptionally useful and often a preferred method of chiral alcohol synthesis.[19] To circumvent the limitations of the dihydroxylation chemistry, we envisioned that a biocatalytic reduction of α-hydroxyketone **11**[20] would provide efficient access to the key diol intermediate **2** (Scheme 3). [21]

Scheme 3. Chiral diol synthesis via enzymatic ketone reduction

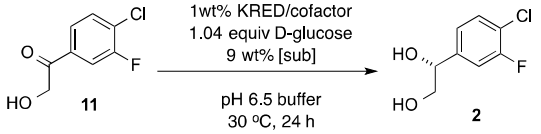

We initiated a focused screen for the asymmetric reduction of α-hydroxyketone **11** based on our prior experience with biocatalysis on similar substrates.[22] Active (*R*)-enantioselective KREDs were screened, applying two different cofactor-recycling systems. One utilized 2-propanol (Table 1) while the other used D-glucose (Table 2) as the terminal reductant. Both reagents were suitable for the use of the cofactors, NADH

and NADPH. In the latter case, an auxiliary enzyme, glucose dehydrogenase (GDH) was required for cofactor regeneration.

Table 1: Enzymatic ketone reduction with 2-propanol as reductant[a]

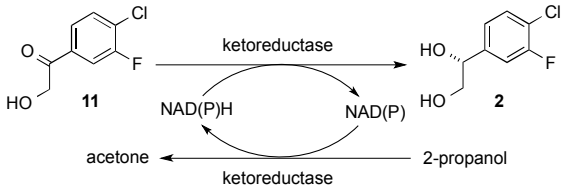

Entry	Enzyme	% Conversion	% ee
1	P2-G03	99.4	99.2 (*S*)
2	P3-B03	11	94.6 (*R*)
3	P3-G09	5.8	84.0 (*R*)
4	P3-H12	30.4	97.9 (*R*)
5	NADH-112	10.3	92.5 (*R*)
6	A131	1.7	56.9 (*R*)

[a] Screening conditions: **11** (0.053 μmol), 2 mM $MgCl_2$, 0.1 M potassium phosphate buffer, pH 7.2; NAD or NADP s/c = 100; enzyme s/e = 10; 5% (v/v) 2-propanol; 5% (v/v) acetonitrile ; rt.

While the single-enzyme system resulted in low conversions or formation of the undesired (*S*)-enantiomer (Table 1), KRED NADH-112 with a D-glucose / GDH recycling system was identified as a highly-efficient catalyst, producing the desired diol **2** with >99% ee and 100% conversion (Table 2, entry 5). The screening result was first confirmed on gram scale at a 5% (w/v) concentration where the reaction was completed in 3 days at ambient temperature, producing **2** in 98% isolated yield and >99.9% ee. Further optimization of the reaction conditions allowed the substrate concentration to be increased to 10% (w/v). The reaction temperature was increased to 30 °C in order to shorten the conversion time to less than 24 h.

Table 2: Enzymatic ketone reduction with D-glucose as a reductant[a]

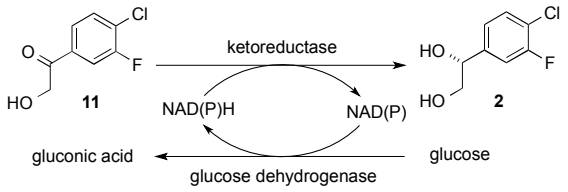

Entry	Enzyme	% Conversion	% ee
1	P2-G03	99.8	100 (*S*)
2	P3-B03	2.7	71.5 (*R*)
3	P3-G09	0.9	40.8 (*R*)
4	P3-H12	12.4	95.4 (*R*)
5	NADH-112	98	99.5 (*R*)
6	A131	5.7	85.4 (*R*)

[a] Screening condition: **11** (0.1 μmol), 2 mM $MgCl_2$, 0.1 M potassium phosphate buffer, pH 7.2; 0.25 M D-glucose; GDH-105 s/e = 100 and NAD or NADP s/c = 100; enzyme s/e = 5; rt.

Methanesulfonate Formation. A two-step, one-pot procedure was developed to synthesize methanesulfonate **4** (Scheme 4). Selective protection of the primary alcohol with a TBS group proceeded smoothly with minimal formation of the over-protected by-product. We initially used Et_3N with a catalytic amount of DMAP as base for both steps. The reaction was heterogeneous in dichloromethane at a 7% (w/v) concentration and went to completion in over 12 h at 20 °C. Substitution of Et_3N with Hünig's base allowed reaction completion in 2 h at the same temperature and remained homogenous at a 20% (w/v) concentration. Methanesulfonyl chloride was then introduced to the reaction mixture to yield **4** in >98A% HPLC purity. Due to the instability of **4**, after work-up, the crude solution was taken to the next step without further purification.

Scheme 4. One-pot synthesis of methanesulfonate 4

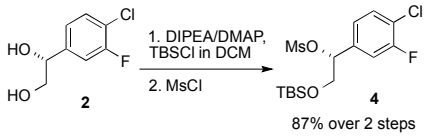

S_N2 Displacement. With access to the methanesulfonate **4** secured, we turned our attention to the S_N2 reaction with pyridone **5** (Scheme 5).[23] In the original process, the reaction produced *N*-alkylation adduct **6** in modest 50-60% yields along with >20% of the undesired *O*-alkylation by-product **12**.

Scheme 5. S_N2 reaction of methanesulfonate 4 and pyridone 5

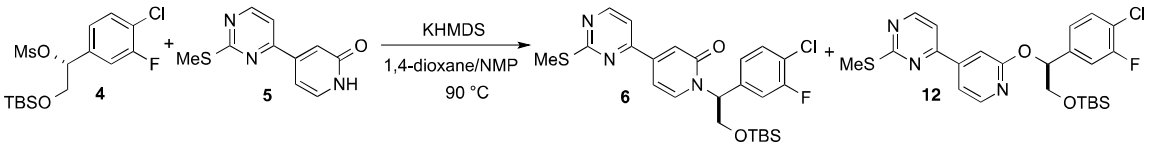

A series of reaction conditions were evaluated to improve the regioselectivity in the alkylation reaction. Weak organic (TMG, DABCO, 2,6-lutidine and DMAP) and inorganic bases (alkali metal fluorides, carbonates and phosphates) resulted in <60% conversions to **6** in 24 h. In a few cases (DBU and PPh_3 / DIAD), the reaction went to completion, but favored the undesired *O*-alkylation by-product **12**. While some strong bases (metal hydride and alkali metal *tert*-butoxide) afforded messy reaction profiles, metal hexamethyldisilazide (MHMDS) variants in general led to a cleaner reaction and favored formation of the desired *N*-alkylation product **6**. The counter-ion effect on the regioselectivity of the S_N2 reactions was then investigated (Table 3). By comparison of lithium, sodium and potassium, it appeared that as the size of counter-ion increased, the selectivity was improved. However, the cesium salt of pyridone **5** deviated from this trend and gave a low selectivity.

Table 3. Counter-ion effect on regioselectivity[a,b]

Entry	MHMDS	% Conversion[b]	*N* vs *O* ratio 6:12[b]
1	LiHMDS	90	71:29
2	NaHMDS	>95	79:21
3	KHMDS	>95	84:16
4	Cs salt of **5**[c]	92	73:27

[a] Reaction conditions: 1.0 equiv of **4** (5 mmol), 1.1 equiv of **5** (5.5 mmol), 1.1 equiv of MHMDS in THF, 80 °C for 8 h; [b] Conversion and selectivity were monitored by HPLC analysis. [c] Cs salt of **5** was prepared by mixing a 1:1 ratio of CsOH solution and **5** followed by precipitation with CH_3CN.

Solvent also played a critical role in the regioselectivity of the S_N2 reaction (Table 4). Although polar solvents allowed for the reaction to go to completion in a few hours, there was no differentiation between two alkylation pathways, resulting in 1:1 mixtures of both regioisomers (entries 1-3). On the other hand, non-polar solvents in general enable a reaction with reasonable selectivity (entries 4-6). However, due to the low solubility of **4**, thick slurries were obtained and made the agitation challenging. The addition of 5-10% NMP as a co-solvent helped to alleviate the mixing issue. We observed that the reaction stalled at ~90% conversion in THF / NMP or toluene / NMP and required extended reaction times to achieve full conversion. The reaction in 1,4-dioxane with 5% NMP gave a very thin slurry. As a result, full conversion was obtained in 18 h with an acceptable level of *N* vs *O* selectivity (entry 7). Fortunately, the *O*-alkylated regioisomer **12** was purged below 0.5A% HPLC after crystallization of **6** from *n*-heptane. Under all those reaction conditions, a complete inversion of stereochemical

configuration of the benzylic chiral center was observed during the displacement reaction and no erosion of enantiomeric excess could be detected based on HPLC analysis of the crude reaction mixture.

Table 4. Solvent effect on the conversion and regioselectivity[a]

Entry	Solvent	Co-solvent	Temperature (°C)	% Conversion[b]	*N* vs *O* ratio 6:12[b]
1	NMP	-	100	100	50:50
2	DMF	-	100	100	49:51
3	MeCN	-	70	100	58:42
4	toluene	10% NMP	100	89	84:16
5	THF	10% NMP	70	95	88:12
6	1,4-dioxane	-	70	93	89:11
7	1,4-dioxane	5% NMP	70	100	87:13

[a] Reaction conditions: 1.0 equiv of **4** (5 mmol), 1.1 equiv of **5** (5 mmol), 1.1 equiv of KHMDS in THF; at the indicated temperature for 18 h; [b] Conversion and selectivity were monitored by HPLC analysis.

Sulfone Synthesis via Oxidation. Conversion of sulfide to the sulfone was initially accomplished with 3-chloroperbenzoic acid (*m*-CPBA) in dichloromethane (Scheme 6). Sulfone **7** was isolated in 80-85% yield as a pure crystalline solid. These reaction conditions were then scaled up to produce the first few batches of **7**. Although the reaction yields were consistently high, pyrimidine *N*-oxide impurity **13** (~1A% HPLC) was observed and led to the corresponding *N*-oxide impurity in the final API (~0.5A% HPLC).[24] Unfortunately, there was no purge of API *N*-oxide in the final salt formation

and recrystallization steps. The rejection of **13** after the oxidation step was attempted via a crystallization of **7** in THF / *n*-heptane but the purge efficiency proved to be quite low (less than one-fold). As a consequence, four recrystallizations were required to reduce the level of **13** from 0.8% to below 0.15%. In addition to the impurity issue, the *m*-CPBA reaction was deemed to be an environmentally unfavorable process due to a low atom economy with formation of a benzoic acid by-product and use of undesirable dichloromethane as reaction solvent.

Scheme 6. Sulfone synthesis via an *m*-CPBA oxidation

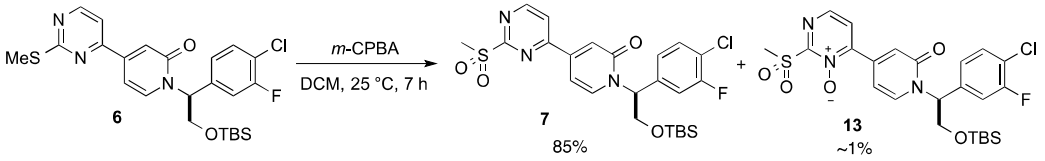

Table 5. Solvent effect on sulfide oxidation[a]

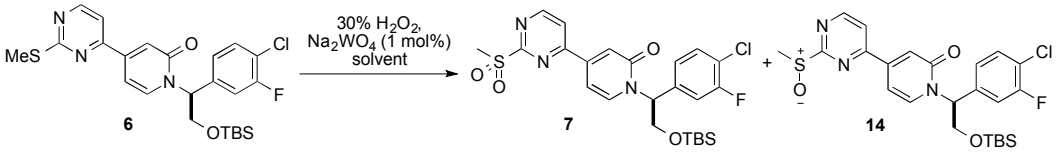

Entry	Solvent	Time (h)	A% HPLC 6	A% HPLC 14	A% HPLC 7
1	EtOH	7	15	18	67
2	EtOH / H_2O (9:1)	3	1	1	98
3	NMP / H_2O (9:1)	22	28	1	71
4	DMF / H_2O (9:1)	22	10	5	85
5	THF / H_2O (9:1)	22	6	3	91
6	MeCN / H_2O (9:1)	6	1	1	98
7	*n*-PrOH / H_2O (50:1)	2	1	0	>99

[a] Reaction conditions: 1.0 equiv of **6** (5 mmol), 2.2 equiv of 30 wt% H_2O_2, 1 mol% of Na_2WO_4, in 10 mL/g of solvent

As an alterative to *m*-CPBA, aqueous hydrogen peroxide has been shown in the literature to be one of cheap and green oxidants.[25] Sulfone synthesis via a molybdate- or tungstate-catalyzed sulfide oxidation with aqueous hydrogen peroxide has been well documented.[26-28] We then quickly evaluated the efficiency of Na_2WO_4-catalyzed oxidation of sulfide **6** with 30% aqueous H_2O_2 in a variety of solvents (Table 5). It was found that EtOH (entry 1) gave an incomplete conversion after 7 h. Reactants were not completely soluble in this solvent system, resulting in a heterogeneous reaction. With the addition of 10% (v/v) of water, all reagents were soluble and full conversion was observed after 3 h (entry 2). Polar aprotic solvents NMP, and DMF (entries 3 and 4) were found to have greater solubility but significantly decreased the rate of reaction, resulting in incomplete reaction after extended periods of time. Aqueous THF or acetonitrile (entries 5 and 6) were found to have excellent solubility of reagents and products, resulting in a 90-98% conversion. *n*-PrOH with 2% (v/v) of water (entry 7) was identified to be optimal, allowing for >99% conversion in 2 h.

Figure 2. Observed impurities in sulfide oxidation with H_2O_2

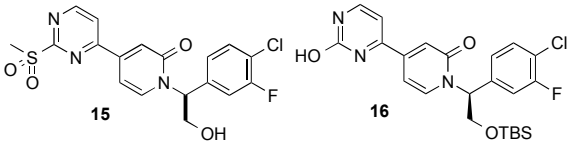

Due to the acidic nature of H_2O_2,[29] desilylated sulfone by-product **15** was observed within 2 h reaction time at up to 3.2A% HPLC (Table 6, entry 1). A stress test indicated that nearly full desilylation was obtained after 18 h under the reaction conditions (entry 2). A base screen was performed to suppress formation of **15** (Figure 2). While other bases

had either a low efficiency to minimize **15** or formed more hydrolysis impurity **16** (entries 3-5), we found that 2,6-lutidine (entry 6) was efficient to minimize desilylation without significantly increasing the level of **16**.

Table 6. Base additive to minimize desilylation and hydrolysis impurities[a]

Entry	Base	mol%	Time (h)	A% HPLC 15	A% HPLC 16
1	-	-	2	3.2	0.50
2	-	-	18	95	0.50
3	iPr_2EtN	10	2	8	0.50
4	K_2CO_3	10	2	1.4	3.0
5	KOAc	10	2	2.5	0.90
6	2,6-Lutidine	10	2	0.28	0.53

[a] Reaction conditions: 1.0 equiv of **6** (5 mmol), 2.2 equiv of 30 wt% H_2O_2, 1 mol% of Na_2WO_4, in 10 mL/g of *n*-PrOH / H_2O (50:1)

It is well known that there are potential process hazards associated with a tungstate-catalyzed oxidation with hydrogen peroxide. This transformation is susceptible to exothermic decomposition of H_2O_2 leading to runaway reactions and potential evolution of oxygen. The reaction safety aspects for a tungstate-H_2O_2 oxidation system have been described in some recent publications.[30,31] With optimal reaction conditions established, we then focused on the reaction safety and scalability, addressing potential issues with heat and peroxide accumulation in the oxidation reaction.

Two reaction conditions were examined. When H_2O_2 was charged to the reaction mixture at 40 °C over 2 h, 45% conversion of sulfide **6** was observed at the end of the addition with formation of a mixture of sulfone **7** and sulfoxide intermediate **14**. This result indicated a high level of peroxide accumulation after charging as the reaction went

to completion within additional 4-5 hours. Reaction calorimetry was carried out to measure the enthalpy of the reaction in a reaction calorimeter (RC1), revealing a significant heat accumulation after charging (Table 7). This translated to a high adiabatic temperature rise of 12.7 °C. In contrast, when H_2O_2 was added to a reaction mixture at 80 °C with the same addition time, >95% conversion of sulfide to sulfone was observed. As a result of the faster reaction rate, minimal H_2O_2 was accumulated in the reaction and the post-addition enthalpy was significantly reduced.

Table 7. Temperature effect on heat and H_2O_2 accumulation[a]

Reaction and thermal parameter	Reaction temperature 40 °C	Reaction temperature 80 °C
Conversion of sulfide at the end of addition	45%	>95%
Overall enthalpy of reaction	-444.1 kJ/mol	-503.5 kJ/mol
Enthalpy of reaction during H_2O_2 addition	-282 kJ/mol	-475.8 kJ/mol
Enthalpy of reaction post-addition	-162.1 kJ/mol	-27.7 kJ/mol
Adiabatic temperature rise post-addition	12.7 °C	3.1 °C

With a safe operation procedure in place, the oxidation was successfully demonstrated and upon reaction completion, residual H_2O_2 was quenched with an

aqueous sodium ascorbate solution at 80 °C. The crystalline sulfone product was directly precipitated from the reaction mixture with the addition of water as an anti-solvent. The crystallization was found to be effective in purging impurities **15** (3×) and **16** (>10×). The product was obtained in 87% isolated yield with *N*-oxide impurity **13** controlled below the detection limit (LOD <0.05A% HPLC).

Sulfone Displacement with Aminopyrazole (S_NAr Step). S_NAr displacement (Scheme 7) was initially carried out in DMF and employed Cs_2CO_3 as a base. The reaction suffered from a modest conversion at ambient temperatures and a complex reaction profile at 80 °C. The average yield of the reaction was approximately 60%. The modest isolated yields were due to the formation of significant quantities of by-product **17** (Figure 3) via hydrolysis of the sulfone functionality (Table 8, entry 1). To improve the reaction yield, the reactivity and selectivity issues would have to be resolved. We speculated that the nucleophilicity of aminopyrazole **8** could be increased by a direct deprotonation of **8** with a strong base. On the other hand, the formation of a high level of **17** could be attributed to a high concentration of metal hydroxide in the reaction solution, leading to a competitive displacement of the sulfone. In contrast to the high solubility of CsOH in DMF, LiOH has a much lower solubility in THF. We surmised that LiHMDS in THF would be a good combination to not only increase the reactivity of **8** as an anion but also reduce the hydrolysis side reaction.

Scheme 7. Sulfone displacement with aminopyrazole

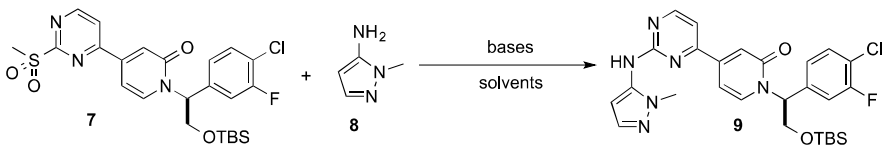

Figure 3. Observed impurities in S_NAr step

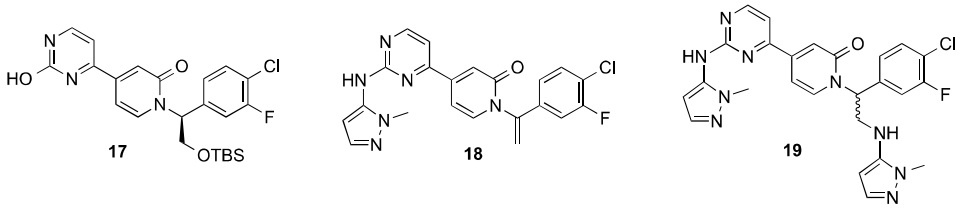

As shown in Table 8, when LiHMDS was employed as a base, the reaction rate was dramatically increased. At ambient temperature, the reaction went to completion immediately after the addition of base (entry 2). By comparison, <90% conversion was obtained after 24 h using the original procedure (entry 1). The change in conditions also decreased the level of hydrolysis by-product **17** from 15-20A% HPLC to 3A% HPLC. Formation of **17** was further reduced to below 1A% HPLC after the reaction temperature was decreased to –30 °C. In addition, the decrease in reaction temperature had no noticeable impact on the reaction rate (entry 3). When 10 mol% of water was added to the reaction solution, the same level of **17** was observed (entry 4) as that under the anhydrous conditions. This observation indicated the same concentration of LiOH under both anhydrous and wet conditions. This is presumably due to a low solubility of LiOH in THF, leading to a precipitation of LiOH out of the saturated solution and a negligible impact on the impurity formation.

Table 8: Base and solvent effect on S_NAr[a,b]

Entry	Base	Solvent	Temperature (°C)	Time	% Conversion	A% HPLC 17
1	Cs_2CO_3	DMF	25	24 h	<90	15-20
2	LiHMDS	THF	25	10	100	3

				min		
3	LiHMDS	THF	-30	10 min	100	<1
4	LiHMDS	THF with 10 mol% water	-30	10 min	100	<1

[a] Reaction conditions: 1.0 equiv of **7** (5 mmol), 1.2 equiv of **8** (6 mmol), 2.1 equiv of base at the indicated temperature; [b] Reactions were monitored by HPLC analysis.

Although employing a strong base resulted in improved conversions and reaction profiles, two new impurities were introduced. Due to a fairly acidic proton at the chiral benzylic position**,** one impurity **18** (Figure 3) was generated through an elimination pathway when using excess LiHMDS. The other impurity **19** (Figure 3) was derived from **18** through the subsequent addition of **8**. The stoichiometry of base is critical of achieving full conversion while minimizing the formation of **18** and **19** (Table 9). The NH proton of the product **9** is the most acidic site in the reaction mixture and acts as an irreversible base sink. As a result, only 50% conversion was observed when 1 equivalent of LiHMDS was applied (entry 1). Since the NH proton of **8** is more acidic than the benzylic proton, an excess of **8** is able to serve as a buffer for the over-charged base. When slight excesses of LiHMDS were employed and trapped by **8**, no significant by-products were formed (entry 2). In contrast, when large excesses of base were charged and cannot be completely consumed by **8**, a significant amount of **18** and **19** were observed (entry 3).

Table 9. Impact of LiHMDS equivalents on conversion and impurity formation

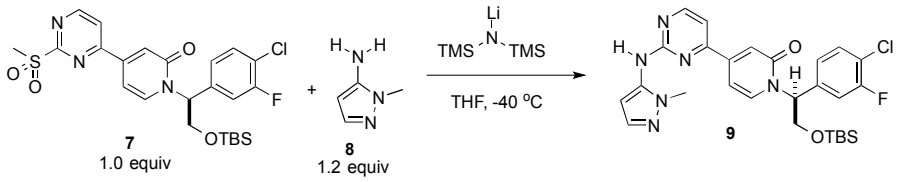

Entry	Equivalent of LiHMDS	% Conversion	A% HPLC 18[a]	A% HPLC 19[a]
1	1.0	~50	-	-
2	2.1	100	1.1	1.2
3	2.3	100	6.5	4.1

[a] Reaction conditions: 1.0 equiv of **7** (5 mmol), 1.2 equiv of **8** (6 mmol), indicated amount of LiHMDS at –40 °C; [b] Reactions were monitored by HPLC analysis.

The level of both impurities **18** and **19** can be further reduced in the downstream benzenesulfonate salt formation and API recrystallization steps. The measured purge factors of **18** were 3× in the salt formation step and 2× in the final recrystallization step. The rejections of **19** in those two steps were more efficient. To purge individual impurities below the GMP specifications at the end, the level of impurity **18** needed to be controlled below 0.5% in the S_NAr step. This requirement led to further optimization of bases, solvents and temperatures (Table 10). The base screen indicated that LiHMDS was the best choice (entry 1). Other strong bases, KHMDS, NaHMDS or Li*O*t*Bu resulted in either a higher level of both **18** and **19** or formation of other impurities (entries 2-4). Co-solvents had a significant impact on the level of impurities. While use of the polar co-solvent NMP was unsuccessful to reduce the level of both impurities (entry 5), non-polar co-solvent, MTBE, toluene and 2-MeTHF improved the reaction purity profile (entries 6-8). 0.60% of **18** and <0.1% of **19** was observed in the reaction when employing LiHMDS

in 2-MeTHF (entry 9). The level of both impurities can be further reduced when the reaction temperature was decreased to –25 °C (entry 10).

Table 10. Optimization of Conditions for S_NAr[a]

Entry	Base	Solvent / additive	Temp. (°C)	A% HPLC 9[b]	A% HPLC 18[b]	A% HPLC 19[b]
1	LiHMDS[d]	THF	5	88	4.2	2.1
2	KHMDS[d]	THF	5	42	11	21
3	NaHMDS[d]	THF	5	63	14	9.0
4	LiO*t*Bu[d]	THF	5	58[c]	-	-
5	LiHMDS[d]	THF / NMP 20:1 (v/v)	5	80	5.3	4.9
6	LiHMDS[d]	THF / MTBE[g] 1:1 (v/v)	5	91	1.1	0.12
7	LiHMDS[e]	THF[h]	5	92	2.8	1.1
8	LiHMDS[d]	THF / 2-MeTHF[g] (1:1 v/v)	5	89	2.7	1.5
9	LiHMDS[f]	THF[i]	5	94	0.60	<0.1
10	LiHMDS[f]	THF[i]	–25	96	0.31	n/d

[a] Reaction conditions: 1.0 equiv of **7** (5 mmol), 1.2 equiv of **8** (6 mmol), 2.1 equiv of base in the indicated solvent, 10 mL/g of the final reaction volume after addition of a base solution; [b] Reactions were monitored

by HPLC analysis; [c] The reaction contained 42A% HPLC of by-product with *t*-butyloxide displacement of sulfone functionality; [d] MHMDS or MO*t*Bu in THF (1.0 M); [e] LiHMDS in toluene (1.0 M); [f] LiHMDS in 2-MeTHF (0.5 M). [g] Final solvent ratio THF:MTBE or THF:2-MeTHF = 1.7:1 (v/v). [h] Final solvent ratio THF:toluene = 3:1 (v/v). [i] Final solvent ratio THF:2-MeTHF = 1.5:1 (v/v).

Scheme 8. Telescoped desilylation and benzenesulfonate salt formation

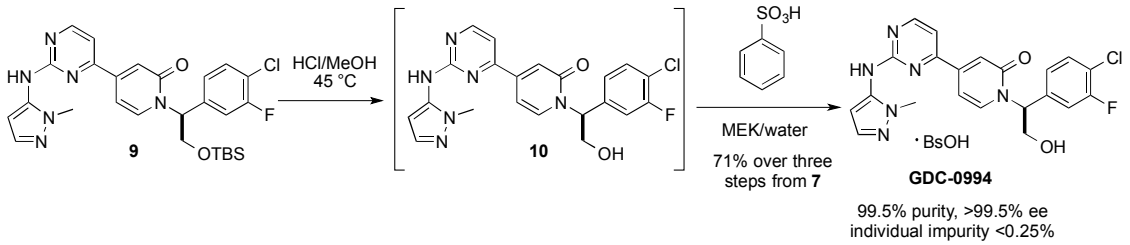

Telescoped Desilylation and Benzenesulfonate Salt Formation. No crystalline forms were found for the freebase of GDC-0994 **10** following extensive screening. After salt screens, a few crystalline salt forms were identified with strong acids (HCl, *p*-toluenesulfonic acid and benzenesulfonic acid). Among them, the benzenesulfonate salt of GDC-0994 possessed superior stability and very low hygroscopicity. As a result, it was identified as an appropriate polymorph for further development.

The desilylation was initially achieved using HCl in MeOH at 45 °C (Scheme 8). The reaction typically proceeded to 70-80% conversion within the first 3 h, but required more than 10 h to go to completion. After the reaction was finished, an azeotropic distillation was carried out to facilitate the removal of the corresponding by-product, tert-butyl-methoxy-dimethylsilane, before quenching. The content of MeOH in EtOAc was then controlled at 15–20 wt% to ensure a good solubility of GDC-0994•HCl salt in the organic phase, while minimizing aqueous losses. Since the formation of benzenesulfonate salt involved 1 equivalent of benzenesulfonic acid, there was a quality concern associated with the introduction of the genotoxic impurity methyl benzenesulfonate as a byproduct

from reaction of the acid in methanol. MeOH levels were reduced to below 0.3A% GC through concentration and solvent swap before the benzenesulfonate salt formation step.

GDC-0994•benzenesulfonate has a low solubility in methyl ethyl ketone (MEK) (<5 mg/mL). However, the impurity rejection for both impurities **18** and **19** using a pure organic solvent was minimal. Introduction of water as a co-solvent enabled significant reduction of both impurities.[32] Since over 20% mass loss was observed with 5% of water in MEK, 3-4% of water in MEK was chosen for the salt formation step to balance the recovery of API and the purge of impurities. GDC-0994•benzenesulfonate salt was isolated in 71% yield over three steps and in 99.6 A% HPLC and >99.5% ee purity.

Scheme 9. One-pot desilylation and benzenesulfonate salt formation

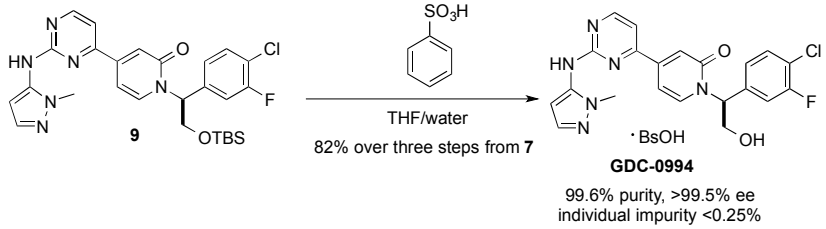

One-pot Desilylation and Benzenesulfonate Salt Formation using Benzenesulfonic Acid. While the end game process via the telescoped deprotection / salt formation provided GDC-0994 API efficiently, we realized that the whole process could be further streamlined by the removal of unnecessary unit operations. Since desilylation only required a catalytic amount of acid, we envisioned that benzenesulfonic acid could serve a dual purpose as a catalyst for deprotection and acid for salt formation. After acid-catalyzed desilylation, the crystalline benzenesulfonate salt would precipitate out of the reaction solution. As a result, a freebasing step and lengthy solvent switches could be removed.

Although the genotoxic impurity methyl benzenesulfonate was well controlled and

closely monitored in the telescoped process, it is ideal to avoid alcoholic solvents in the salt formation step and completely eliminate genotoxic impurity concerns. After the S_NAr reaction in the optimal THF / 2-MeTHF solution was completed, the solvents were swapped to THF / water for the subsequent desilylation and salt formation (Scheme 9). Our initial attempts to perform a crystallization-driven reaction to form the API benzenesulfonate salt in THF with a lower water content (<3 wt%) were successful but resulted in an uncontrolled precipitation of the product. This led to unreacted intermediate **9** being trapped in the solids and a high level of **9** (1-2A% HPLC) in the crude API. To alleviate this issue we decided to perform the deprotection reaction in a homogeneous solution with a higher water content in THF (10 wt%). After complete deprotection, excess water was removed through azeotropic distillation. The solvent composition was then adjusted into the metastable zone before seeds were introduced for a controlled crystallization. As a result, the API was obtained with 82% isolated yield over 3 steps and excellent purity (>99.5A% HPLC and >99.5% ee, no individual impurities were observed over 0.25%).

Recrystallization of crude API. Although the purity of crude API was high enough to meet our specifications, a recrystallization was developed and implemented to further ensure API quality and a controlled unimodal distribution of particle size [d (0.5) < 50 micron]. The crude GDC-0994•benzenesulfonate salt was dissolved at 78 °C in EtOH after slowly introducing water to ~10 wt%. After a hot polish filtration, seeds were charged at 60 °C to induce crystallization. The water content of the solution was then adjusted to 2-3 wt% via an azeotropic distillation at 60 °C to maximize recovery. The recrystallization offered decent purging of impurities **17** (>10×), **18** (2×) and **19** (3×).

GDC-0994•benzenesulfonate API was isolated in 89% yield.

3. CONCLUSION

In summary, an efficient and scalable synthetic route to the ERK inhibitor, GDC-0994•benzenesulfonate was developed and demonstrated on a multiple kilogram scale. The API was prepared in 7 steps, 41% overall yield and high purity of >99.5A% HPLC and >99.5% ee (Scheme 10). A highly enantioselective enzymatic ketone reduction was developed as an efficient approach to the chiral diol intermediate. The performance and regioselectivity of the pyridone S_N2 reaction was improved from ~50% yield (*N* vs *O* ratio 80:20) to 74% yield (*N* vs *O* ratio, 89:11) with careful selection of base and solvent screens. The sulfide oxidation with *m*-CPBA was replaced by green and efficient tungstate-catalyzed oxidation with hydrogen peroxide. The reaction safety of the oxidation was evaluated to achieve a safe and robust process. The S_NAr displacement reaction was optimized to control levels of impurities observed in the final API. The end game steps were streamlined with development of a telescoped S_NAr / desilylation / benzenesulfonate salt formation process. Finally, development of the API recrystallization enabled further purging of impurities.

Scheme 10. Practical Synthesis of GDC-0994

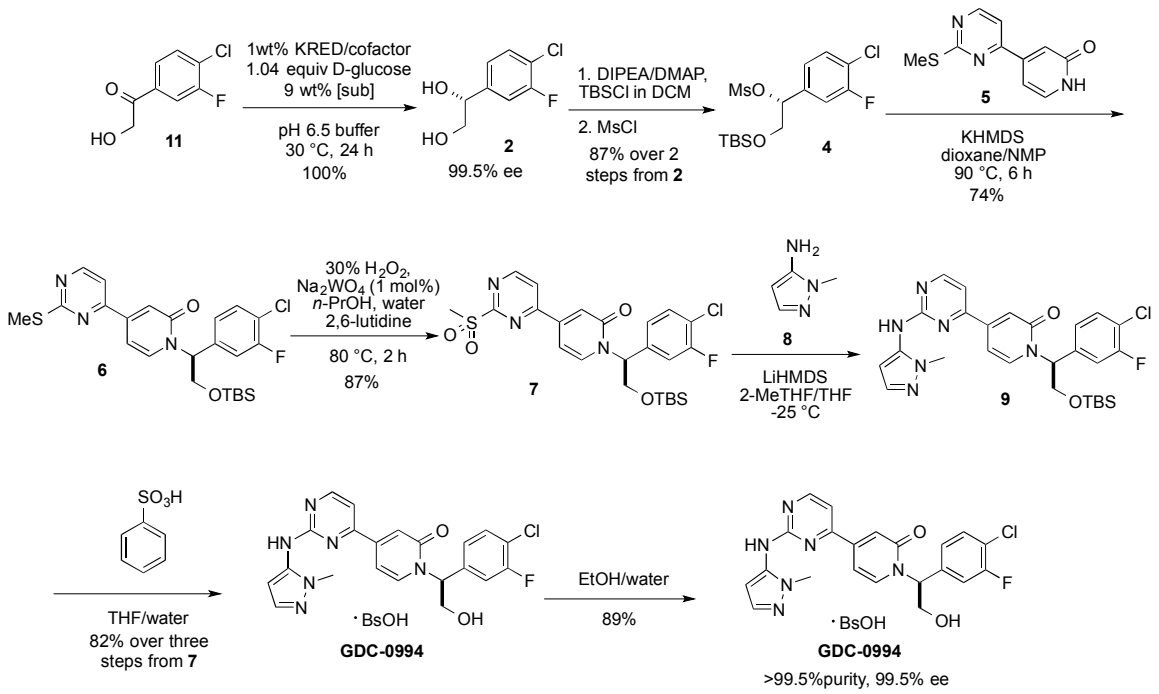

4. EXPERIMENTAL SECTION

General. All commercially available reagents and solvents, including anhydrous solvents, were used without further purification. Assay yields were obtained using analytical standards prepared by recrystallization or preparative chromatography. All isolated yields reflect correction for purity based on HPLC analyses or qNMR assays. ^{1}H (400 MHz), ^{13}C (100 MHz), and ^{19}F (282 MHz) NMR spectra were recorded at room temperature (RT) on a Bruker spectrometer. Chemical shifts (δ) are expressed in parts per million (ppm) relative to the corresponding deuterated solvent peak. HPLC analyses were conducted on an Agilent 1200 series (Agilent Zorbax SB-Phenyl column (150 x 4.6 mm, 3.5 μm); and mobile-phase gradients consisting of 0.05% TFA in water and 0.05% TFA in acetonitrile) or (Waters Xbridge Phenyl column (150 x 4.6 mm, 3.5 μm); and mobile-phase gradients consisting of 0.05% TFA in water and 0.05% TFA in acetonitrile). Chiral HPLC analyses were conducted on an Agilent 1200 series (Chiralpak IA column (250 x 4.6 mm, 5 μm); isocratic mobile phase 80% *n*-hexane and 20% ethanol). Analytical characterizations were obtained on materials that were representative or purified for that purpose.

(*R*)-1-(4-chloro-3-fluorophenyl)ethane-1,2-diol (2). To a 500 L reactor under N_2 was charged water (150 kg), 4-morpholine ethanesulfonic acid (0.90 kg, 4.6 mol) and anhydrous magnesium chloride (0.030 kg, 0.3 mol). After a clear solution was obtained, *n*-heptane (37 kg), **11** (30 kg, 159 mol), D-(+)-glucose monohydrate (34.8 kg, 176 mol) and PEG 6000 (30.0 kg) were charged. The pH of the solution was adjusted to 6.5-7.0 by a 1N aqueous NaOH solution at 28-32 °C. To the resulting solution was charged GDH-105 (0.30 kg), β-diphosphopyridine nucleotide (0.30 kg, 0.45 mol) and KRED-NADH-

112 (0.30 kg). The resulting suspension was stirred at 29-31 °C for 10-12 h while maintaining the pH of the reaction mixture at 6.5-7.0 by the controlled addition of a 1N aqueous NaOH (160 kg). The pH of the reaction mixture was adjusted to 1-2 by the addition of 49% H_2SO_4 (20 kg) to quench the reaction. EtOAc (271 kg) was then added and the mixture was stirred at 20-30 °C for 10-15 min. The mixture was filtered through a pad of celite and the cake was washed with EtOAc (122 kg). The combined organic layers were separated and aqueous layer was extracted with EtOAc (150 kg). The organic layers were combined and washed with water (237 kg). The pH of the mixture was adjusted to 7.0-8.0 by addition of solid $NaHCO_3$. The organic layer was separated, concentrated and then switched to CH_2Cl_2. The crude product was obtained as a CH_2Cl_2 solution (30.9 kg, 100% assay yield, 99A% HPLC purity and >99.5% ee, 7.9 wt% in CH_2Cl_2).

(*R*)-2-((tert-butyldimethylsilyl)oxy)-1-(4-chloro-3-fluorophenyl)ethyl methanesulfonate (4). To a 1000 L reactor under nitrogen was charged with **2** (30.9 kg in 390 kg of anhydrous CH_2Cl_2, 163 mol). The solution was cooled to –5 °C. *Tert*-butylchlorodimethyl silane (26.9 kg, 173 mol) was added in portions at –5 °C. A solution of 4-dimethylaminopyridine (0.995 kg, 3.3 mol) and triethylamine (43 kg, 426 mol) in anhydrous CH_2Cl_2 (135 kg) was added dropwise to the above solution at –5 °C. The reaction solution was warmed to 25 °C over 2.5 h and stirred for 12 h. The obtained solution was cooled to –5 °C. A solution of methanesulfonyl chloride (20.4 kg, 179 mol) in anhydrous CH_2Cl_2 (135 kg) was added to the above solution over 4 h and the temperature was controlled below 0 °C. After stirring at 5 °C for 2 h, the reaction was washed with water (229 kg), followed by 5 wt% aqueous citric acid (236 kg), 2 wt%

$NaHCO_3$ aqueous solution (228 kg) and finally water (228 kg). The resulting CH_2Cl_2 solution was dried over anhydrous Na_2SO_4 (1.5 kg), filtered, rinsed with CH_2Cl_2 (38 kg) and concentrated in vacuo below 15 °C to afford crude **4** as a CH_2Cl_2 solution (54.8 kg in 206 kg of CH_2Cl_2, 94.9A% HPLC purity, 26.6 wt% and 88.0% assay yield, KF = 0.01%).

(*S*)-1-(2-((*tert*-butyldimethylsilyl)oxy)-1-(4-chloro-3-fluorophenyl)ethyl)-4-(2-(methylthio)pyrimidin-4-yl)pyridin-2(1*H*)-one (6). In a 1000 L reactor, a solution of **4** (197.9 kg, 26.6% assay, 130 mol) in CH_2Cl_2 was switched to THF (301 kg) to remove residual CH_2Cl_2 (KF = 0.01% and residual CH_2Cl_2 = 1%). The resulting solution was then concentrated to 3 volumes and transferred to a drum. To a 1000 L reactor was charged **5** (27.1 kg, 96.1 wt% assay solid, 119 mol), anhydrous NMP (14 kg) and anhydrous 1,4-dioxane (417 kg). A solution of KHMDS (124 kg, 1M in THF) was added drop-wise below 40 °C under N_2. The mixture was stirred at 25-40 °C for 3 h. The pretreated solution of **4** in THF was added while maintaining the temperature below 40 °C. The reaction solution was warmed to 80-90 °C and stirred at the same temperature for 6 h. The reaction mixture was concentrated to 70 L to remove dioxane at 40 °C in vacuo. To the reaction mixture was added 547 kg of CH_2Cl_2 and 160 kg of water at 15 °C. The pH of the solution was adjusted to 6.0 with 30 wt% citric acid aqueous solution (6.4 kg). After the phase separation, the CH_2Cl_2 layer and middle emulsion layer were filtered through a celite (9 kg) pad. The organic layer was separated and washed with 3 wt% Na_2SO_4 (2 x 214 kg). The combined aqueous layers were back-extracted with CH_2Cl_2 (168 kg). The combined organic layers were filtered through a silica gel pad (15 kg) and the pad was washed with CH_2Cl_2 (134 kg). The combined filtrates were concentrated to 80 L. The solution was then switched with *n*-heptane in three portions (180 kg + 84 kg +

134 kg) to remove CH_2Cl_2 and concentrated to 80 L (2 volumes) at 30 °C under reduced pressure. The slurry was cooled to 0-10 °C and stirred at the same temperature for 10 h. The solid was isolated and dried at 35-45 °C for 16 h to afford **6** (49.6 kg, 74% isolated yield, 93.9 wt% NMR assay, 95.5A% HPLC purity and >99.5% ee) as a brown solid. mp 124.6 °C; ^{1}H NMR (400 MHz, $CDCl_3$): 8.64 (d, *J* = 5.2 Hz, 1H), 7.44 (d, *J* = 7.6 Hz, 1H), 7.41 (t, *J* = 8.0 Hz, 1H), 7.33 (d, *J* = 5.2Hz, 1H), 7.30-7.27 (m, 2H), 7.14 (d, *J* = 8.4 Hz, 1H), 6.84 (dd, *J* = 7.6, 2.0 Hz, 1H), 6.22 (t, *J* = 4.0 Hz, 1H), 4.33 (dd, *J* = 11.6, 4.0 Hz, 1H), 4.21 (dd, *J* = 11.6, 4.0 Hz, 1H), 2.63 (s, 3H), 0.86 (s, 9H), 0.039 (s, 3H), -0.02(s, 3H). ^{13}C NMR (100 MHz, $CDCl_3$): 173.57, 162.52, 160.90, 158.43, 158.24 (d, *J* = 248 Hz), 147.04, 138.31 (d, *J* = 6.5 Hz), 137.20, 131.03, 125.07 (d, *J* = 3.6 Hz), 120.93 (d, *J* = 17.5 Hz), 118.53, 117.0 (d, *J* = 22.1 Hz), 112.44, 103.28, 62.63, 57.88, 25.81, 18.17, 14.33, -5.62, -5.66. ^{19}F NMR (282 MHz, $CDCl_3$) -114.15 (dd, *J* =10.0, 7.6). HRMS calcd for $C_{24}H_{29}ClFN_3O_2SSi$ [M + H] 506.1501, found 506.1490.

(*S*)-1-(2-((*tert*-butyldimethylsilyl)oxy)-1-(4-chloro-3-fluorophenyl)ethyl)-4-(2-(methylsulfonyl) pyrimidin-4-yl)pyridin-2(1*H*)-one (7): Oxidation with *m*-CPBA. To a 1000 L reactor was charged **6** (48.1 kg, 93.9 wt%, 90 mol) and CH_2Cl_2 (664 kg). To the resulting solution was charged *m*-CPBA (39 kg, 169 mol, 75 wt%) in portions while maintaining the temperature below 10 °C. The reaction was stirred at 5-10 °C for 14 h. The reaction mixture was transferred to a second reactor containing a 6 wt% aqueous $NaHCO_3$ solution (620 kg) over 1.5 h at 10-20 °C. The organic layer was separated and the aqueous layer was extracted with CH_2Cl_2 (73 kg). The combined organic layers were added into a 4.5 wt% aqueous $NaHCO_3$ solution (410 kg). To the resulting mixture at 15-20 °C was charged a 9 wt% aqueous $Na_2S_2O_3$ solution (100 kg) drop-wise to consume

residual *m*-CPBA. Both organic and aqueous layers were tested by KI-starch paper and the results showed no residual oxidant. The aqueous layer was separated and extracted by CH_2Cl_2 (82 kg). The combined organic layers were washed with 3 wt% aqueous Na_2SO_4 solution (380 kg). The organic layer was concentrated to 170 L at 40 °C under reduced pressure and then filtered through a 20 kg silica gel pad. The silica pad was eluted with CH_2Cl_2 (1315 kg). The filtrate was concentrated and then switched to a THF solution (120 L, residual CH_2Cl_2 = 5%). To the resulting solution was charged 31 kg of *n*-heptane drop-wise over 2 h at 20-30 °C and then 1.24 kg of crystalline seed of **7**. The resulting suspension was stirred at 25 °C for 30 min before charging an additional 92 kg of *n*-heptane over 3 h at the same temperature. The suspension was stirred at 25 °C for 3 h and then cooled to 10 °C over 3 h. After stirring at 10 °C for 6 h, the solid was filtered and rinsed with a 65 kg mixture of solvents (V_{THF} :$V_{heptane}$ =1:3). The cake was dried at 45 °C for 12 h to afford **7** as a yellow solid (43.9 kg, 99.6A% HPLC purity, >99.5% ee, 97.8% NMR assay purity and 84% isolated yield). mp 156.5 °C; ^{1}H NMR (400 MHz, $CDCl_3$): 9.05 (d, *J* = 5.2 Hz, 1H), 7.91 (d, *J* = 5.2 Hz, 1H), 7.52 (d, *J* = 7.6 Hz, 1H), 7.40 (t, *J* = 8.0 Hz, 1H), 7.30 (d, *J* = 2.0 Hz, 1H), 7.24 (dd, *J* = 10.0, 2.0 Hz, 1H), 7.12 (d, *J* = 8.4 Hz, 1H), 6.90 (dd, *J* = 7.6, 2.0 Hz, 1H), 6.18 (t, *J* = 3.6 Hz, 1H), 4.32 (dd, *J* = 11.6, 4.4 Hz, 1H), 4.20 (dd, *J* = 11.6, 4.4 Hz, 1H), 3.42 (s, 3H), 0.84 (s, 9H), 0.02 (s, 3H), -0.04 (s, 3H). ^{13}C NMR (100 MHz, $CDCl_3$): 166.67, 163.15, 162.14, 160.0, 158.25 (d, *J* = 248 Hz), 145.10, 137.99 (d, *J* = 6.7 Hz), 137.95, 131.11, 124.97 (d, *J* = 3.6 Hz), 121.08 (d, *J* = 17.6 Hz), 119.86, 119.43, 116.91 (d, *J* = 22.1 Hz), 102.84, 62.58, 58.22, 39.24, 25.80, 18.15, -5.60, -5.66. ^{19}F NMR (282 MHz, $CDCl_3$) -113.94 (dd, *J* =10.0, 7.6). HRMS calcd for $C_{24}H_{29}ClFN_3O_4SSi$ [M + H] 538.1399, found 538.1390.

(*S*)-1-(2-((*tert*-butyldimethylsilyl)oxy)-1-(4-chloro-3-fluorophenyl)ethyl)-4-(2-(methylsulfonyl) pyrimidin-4-yl)pyridin-2(1*H*)-one (7): Na_2WO_4-catalyzed oxidation with H_2O_2. To a 2 L cylindrical reactor was charged *n*-PrOH (450 mL), sulfide **6** (180 g, 356 mmol) and the remaining *n*-PrOH (450 mL). To this mixture was added 2,6-lutidine (10 mol%) and the slurry was heated to 80 °C (internal temperature), resulting in a clear solution. Na_2WO_4 (1.2 g 3.56 mmol) in H_2O (18 mL) was added to the reaction mixture. H_2O_2 (30 wt% in H_2O) (88.7 g, 783 mmol) was then added to the reaction mixture dropwise over 1 h. Upon complete addition of H_2O_2, the mixture was allowed to stir at the same temperature for 30 minutes before the reaction was checked by HPLC analysis. Upon completion of the reaction (>98% conversion to sulfone), Sodium ascorbate (10 wt% in H_2O) (180 mL) was added dropwise over 15 minutes. Peroxide levels and pH were checked at this time (0 ppm peroxides and pH ~9). H_2O (180 mL) was added to the reaction mixture maintaining the internal temperature at 80 °C. After the addition, sulfone seeds (1.8 g, 1 wt%) were added to the mixture. H_2O (540 mL) was then added to the reaction mixture dropwise. The resulting mixture was cooled to 65 °C over 2 h, 45 °C over 3 h then 0 °C over 1 h and held at 0 °C for 16 h. The resulting solid was filtered and washed three times with a 50% aqueous EtOH (500 mL). The absence of residual inorganic salts in the filtrate was checked with a conductivity probe (σ <10 μS/cm). Solids were dried *in vacuo* at 40 °C for 72 h, resulting in **7** as a light yellow crystalline solid (166.6 g, 98.9A% HPLC, >99.5% ee and 87% isolated yield).

(*S*)-1-(2-((*tert*-butyldimethylsilyl)oxy)-1-(4-chloro-3-fluorophenyl)ethyl)-4-(2-((1-methyl-1*H*-pyrazol-5-yl)amino)pyrimidin-4-yl)pyridin-2(1*H*)-one (9). To a clean 100 L cylindrical reaction vessel was charged THF (18 kg). With medium agitation,

7 (4.2 kg, 7.8 mol) and **8** (0.91 kg, 9.4 mol) were charged sequentially, followed by the rest of THF (21 kg). At –40 °C, to the resulting thin slurry was added LiHMDS (14.9 kg, 16.7 mol, 1.0 mol/L in THF) slowly and the internal temperature was controlled below -30 °C. After addition, the reaction was held between –35 and –40 °C for 20 min. The reaction was quenched at the same temperature with 19 wt% H_3PO_4 solution (17 kg) slowly and the internal temperature was controlled below 30 °C. The reaction was diluted with EtOAc (17 kg). After the phase separation, the organic layer was washed with 7 wt% H_3PO_4 solution (13 kg) and then with 4 wt% H_3PO_4 solution (10.5 kg). The organic layer was tested to ensure the level of **8** (≤ 20 μg/mL). The organic layer was washed with 2 wt% NaCl solution (16 kg) and a NaCl and $NaHCO_3$ solution (1.7 kg of NaCl, 0.6 kg of $NaHCO_3$ and 8 kg of water). After the phase separation, residual water in the organic solution was removed through an azeotropic distillation with EtOAc to ≤ 0.5% (by KF) and the solution was then concentrated to 20-30 L under vacuum below 50 °C. The solvent was swapped to MeOH using 30 kg of MeOH and then concentrated to 20-30 L for the next step.

(*S*)-1-(1-(4-chloro-3-fluorophenyl)-2-hydroxyethyl)-4-(2-((1-methyl-1*H*-pyrazol-5-yl)amino)pyrimidin-4-yl)pyridin-2(1*H*)-one (10). To the crude solution of **9** in MeOH from the last step was charged HCl in MeOH (9.0 kg, 9.4 mol, 1.25 M in MeOH) at ambient temperature. The reaction was heated to 45 °C for 16 h. The reaction was then concentrated to 20 L under vacuum below 50 °C. To the resulting solution was charged MeOH (35 kg) and the reaction was concentrated to 20 L again under vacuum below 50 °C. The solvent was then switched to EtOAc (40 kg) and concentrated to 20 L. The ratio of MeOH / EtOAc was controlled to 15:85-20:80. After the solution was cooled

below 30 °C, a 6 wt% $NaHCO_3$ solution (18 kg) was charged slowly, followed by EtOAc (34 kg). After the phase separation, the organic layer was washed with water (2 x 8 kg). The organic layer was concentrated to 20 L under vacuum below 50 °C. The solvent was then switched to MEK (35 kg). The level of MeOH was controlled ≤ 0.3%. The solution was concentrated to 20 L under vacuum below 50 °C for the next step.

GDC-0994. The crude solution of **10** in MEK from the last step was transferred to a second 100 L cylindrical reaction vessel through a 1 μm polish filter. In a separate container was prepared a benzenesulfonic acid solution (1.1 kg, 7.03 mol of benzenesulfonic acid, 1.2 kg of water and 3.7 kg of MEK). The filtered crude solution of **10** was heated to 75 °C and to this resulting solution was charged 10% benzenesulfonic acid solution (0.6 kg) through a 1 μm line filter. To the clear solution was charged **GDC-0994** crystalline seed slurry in MEK (0.021 kg of **GDC-0994** crystalline seed and 0.34 kg of MEK). The rest of benzenesulfonic acid solution was then charged through a 1 μm line filter in 2 h. After addition, the slurry was heated at 75 °C for additional 1 h and then cooled to 18 °C in a minimum of 3 h. The resulting thick slurry was agitated at 18 °C for 16 h. The solid was filtered and washed with 1 μm line-filtered MEK/water solution (0.35 kg of water and 7.8 kg of MEK), followed by 1 μm line-filtered MEK (12 kg). The solid was dried at 40 °C for 16 h to afford crude **GDC-0994** (3.5 kg, 74% isolated yield, 99.1A% HPLC purity and 98.9% NMR weight assay).

GDC-0994: Telescoped S_NAr / Desilylation / Salt Formation. To a clean 500 mL cylindrical reaction vessel was charged THF (120 mL). With medium agitation, **7** (20 g, 37.2 mmol) and **8** (4.5 g, 46.7 mol) were charged sequentially, followed by the rest of THF (120 mL). After dissolution in 5 min, the reaction was cooled to –25 °C. To the

resulting solution was added LiHMDS (160 mL 79.9 mmol, 0.5 mol/L in 2-MeTHF) slowly and the internal temperature was controlled below –20 °C. After addition, the reaction was held between –20 and –25 °C for 10 min. The reaction was quenched at the same temperature with 20 wt% H_3PO_4 solution (80 mL) slowly and the internal temperature was controlled below 30 °C. After the phase separation, the organic layer was washed with 5 wt% H_3PO_4 solution (80 mL) and then with 4 wt% H_3PO_4 solution (80 mL). The organic layer was washed with water (2 X 80 mL). After the phase separation, the solution was concentrated to 100 mL. To the resulting solution was charged 100 mL of THF and then benzenesulfonic acid (5.9 g, 37.2 mmol). The reaction mixture was heated to 60 °C for 30 min. After the reaction was concentrated and the solvent was switched with 2 X 200 mL of THF, the water content was tested (<4 wt%). After the solution was warmed to 60 °C, 100 mg (0.5 wt%) of GDC-0994 crystalline seed was charged. The slurry was concentrated to 80 mL at 65 °C and 80 mL of THF was charged dropwise at the same temperature. The slurry was cooled to 15 °C in 4 h and remained at the same temperature for 16 h. The solid was filtered and washed with 1 vol% water in THF (80 mL) and THF (80 m). The solid was dried at 40 °C for 16 h to afford crude **GDC-0994** (18.2 g, 82% isolated yield, 98.9A% HPLC purity and 98.5% NMR weight assay).

Recrystallization of GDC-0994. To a clean 100 L cylindrical reaction vessel was charged EtOH (21 kg). With medium agitation, crude **GDC-0994** (3.5 kg) was charged, followed by the rest of EtOH (9 kg). The thick slurry was heated to 78 °C and water (1.2 kg) was charged until a clear solution was obtained. The hot solution was filtered through a 1μm line filter to a second clean 100 L cylindrical reaction vessel. To the resulting

solution was charged a **GDC-0994** crystalline seed slurry in EtOH (0.018 kg of **GDC-0994** crystalline seed and 0.35 kg of EtOH). The thin slurry was concentrated to 20 L at 60-70 °C under vacuum. The water content of the solution was controlled at 2.0-3.0wt%. The slurry was then cooled to 20 °C over 3 h and agitated at the same temperature for 16 h. The solid was filtered and washed with 1 μm line-filtered EtOH / water solution (0.2 kg of water and 8 kg of EtOH). The solution was introduced in two equal portions. The solid was then washed by 1 μm line-filtered MEK (6 kg). The wet cake was dried under vacuum with a nitrogen sweep at 40 °C for a minimum 12 h to afford **GDC-0994** as a light yellow solid (3.1 kg, 89% isolated yield, 99.6A% HPLC purity, >99.5% ee). mp 197.7 °C; ^{1}H NMR (600 MHz, DMSO-d6): 9.93, (s, 1H), 8.65 (d, *J* = 5.2 Hz, 1H), 7.95 (d, *J* = 7.27 Hz, 1H), 7.63 (m, 2H), 7.62 (d, *J* = 1.5 Hz, 1H), 7.58 (t, *J* = 8.2 Hz, 1H), 7.55 (d, *J* = 5.2 Hz, 1H), 7.44 (dd, *J* = 10.6, 1.9 Hz, 1H), 7.33 (m, 3H), 7.18 (d, *J* = 2.0 Hz, 1H), 7.17 (d, *J* = 2.1 Hz, 1H), 6.90 (dd, *J* = 7.3, 2.1 Hz, 1H), 6.48 (d, *J* = 2.2 Hz, 1H), 5.99 (dd, *J* = 8.1, 5.5 Hz, 1H), 4.17 (dd, *J* = 11.9, 8.2 Hz, 1H), 4.05 (dd, *J* = 11.9, 5.5 Hz, 1H), 3.78 (s, 3H). ^{13}C NMR (150 MHz, DMSO-d6): 161.60, 161.14, 160.02, 159.79, 157.02 (d, *J* = 245 Hz), 148.0, 146.49, 139.53 (d, *J* = 6.0 Hz), 139.04, 136.96, 136.39, 130.66, 128.42, 127.59, 125.38, 124.99 (d, *J* = 3.0 Hz), 118.72 (d, *J* = 18.0 Hz), 117.29, 116.05 (d, *J* = 22.5 Hz), 109.75, 102.79, 98.77, 60.64, 58.68, 35.29. ^{19}F NMR (282 MHz, DMSO-d6) -115.86 (dd, *J* =10.6, 7.8). HRMS calcd for $C_{21}H_{18}ClFN_6O_2$ [M + H] 441.1242, found 441.1245.

ACKNOWLEDGMENTS

We would like to thank Dr. C.J. Venkatramani and Ms. Ila Patel for analytical support, Dr. Alan Deese for help with NMR analysis, Dr. Christine Gu for HRMS analysis, and Dr. Jeffrey Stults for solid state characterization of GDC-0994.

ASSOCIATED CONTENT

Supporting Information Available
^{1}H, ^{13}C, and ^{19}F data of compound **6**, **7**, and **GDC-0994**.

REFERENCES

(1) Robert, P. J.; Der, C. J. *Oncogene* **2007**, *26*, 3291.

(2) Cheng, J. T.; Cobb, M. H.; Baer, R. *Mol. Cell. Biol.* **1993**, *13*, 801.

(3) Robbins, D. J.; Zhen, E. H.; Cheng, M. G.; Xu, S. C.; Ebert, D.; Cobb, M. H. *Adv. Cancer Res.* **1994**, *63*, 93.

(4) Yap, J. L.; Worlikar, S.; MacKerell, A. D. J.; Shapiro, P.; Fletcher, S. *ChemMedChem* **2011**, *6*, 38.

(5) Nissan, M. H.; Rosen, N.; Solid, D. B. *Cancer Disc.* **2013**, *3*, 719.

(6) Samowitz, W. S.; Sweeney, C.; Herrick, J.; Albertsen, H.; Levin, T. R.; Murtaugh, M. A.; Wolff, R. K.; Slattery, M. L. *Cancer Res.* **2005**, *65*, 6063.

(7) Shapiro, P. *Crit. Rev. Clin. Lab. Sci.* **2002**, *39*, 285.

(8) Brose, M. S.; Volpe, P.; Feldman, M.; Kumar, M.; Rishi, I.; Gerrero, R.; Einhorn, E.; Herlyn, M.; Minna, J.; Nicholson, A.; Roth, J. A.; Albelda, S. M.; Davies, H.; Cox, C.; Brignell, G.; Stephens, P.; Futreal, P. A.; Wooster, R.; Stratton, M. R.; Weber, B. L. *Cancer Res.* **2002**, *62*, 6997.

(9) Morris, E. J.; Jha, S.; Restaino, C. R.; Dayananth, P.; Zhu, H.; Cooper, A.; Carr, D.; Deng, Y.; Jin, W.; Black, S.; Long, B.; Liu, J.; DiNunzio, E.; Windsor, W.; Zhang, R.; Zhao, S.; Angagwa, M. H.; Pinheiro, E. M.; Desai, J.; Xiao, L.; Shipps, G.; Hruza, A.; Wang, J.; Kelly, J.; Paliwal, S.; Gao, X.; Babu, B. S.; Zhu, L.; Daublain, P.; Zhang, L.; Lutterbach, B. A.; Pelletier, M. R.; Philippar, U.; Siliphaivanh, P.; Witter, D.; Kirschmeier, P.; Bishop, W. R.; Hicklin, D.; Gilliland, D. G.; Jayaraman, L.; Zawel, L.; Fawell, S.; Samatar, A. *Cancer Disc.* **2013**, *3*, 742.

(10) Aronov, A. M.; Baker, G.; Bemis, G. W.; Cao, J.; Chen, G.; Ford, P. J.; Germann, U. A.; Green, J.; Hale, M. R.; Jacobs, M.; Janetka, J. M.; Maltais, F.; Martinez-Botella, G.; Namchuk, M. N.; Straub, J.; Tang, Q.; Xie, X. *J. Med. Chem.* **2007**, *50*, 1280.

(11) BVD-523; BioMed Valley Discoveries: Kansas City, MO. https://biomed-valley.com/portfolio/bvd-523; https://clinicaltrials.gov/ct2/show/NCT01781429.

(12) Deng, Y.; Shipps, G. W., Jr.; Cooper, A.; English, J. M.; Annis, D. A.; Carr, D.; Nan, Y.; Wang, T.; Zhu, H. Y.; Chuang, C. C.; Dayananth, P.; Hruza, A. W.; Xiao, L.; Jin, W.; Kirschmeier, P.; Windsor, W. T.; Samatar, A. A. *J Med Chem* **2014**, *57*, 8817.

(13) Blake, J. F.; Gaudino, J. J.; De Meese, J.; Mohr, P.; Chicarelli, M.; Tian, H.; Garrey, R.; Thomas, A.; Siedem, C. S.; Welch, M. B.; Kolakowski, G.; Kaus, R.; Burkard, M.; Martinson, M.; Chen, H.; Dean, B.; Dudley, D. A.; Gould, S. E.; Pacheco, P.; Shahidi-Latham, S.; Wang, W.; West, K.; Yin, J.; Moffat, J.; Schwarz, J. B. *Bioorg. Med. Chem. Lett.* **2014**, *24*, 2635.

(14) Aronov, A. M.; Tang, Q.; Martinez-Botella, G.; Bemis, G. W.; Cao, J.; Chen, G.; Ewing, N. P.; Ford, P. J.; Germann, U. A.; Green, J.; Hale, M. R.; Jacobs, M.; Janetka, J.

W.; Maltais, F.; Markland, W.; Namchuk, M. N.; Nanthakumar, S.; Poondru, S.; Straub, J.; ter Haar, E.; Xie, X. *J. Med. Chem.* **2009**, *52*, 6362.

(15) Ward, R. A.; Colclough, N.; Challinor, M.; Debreczeni, J. E.; Eckersley, K.; Fairley, G.; Feron, L.; Flemington, V.; Graham, M. A.; Greenwood, R.; Hopcroft, P.; Howard, T. D.; James, M.; Jones, C. D.; Jones, C. R.; Renshaw, J.; Roberts, K.; Snow, L.; Tonge, M.; Yeung, K. *J. Med. Chem.* **2015**, *58*, 4790.

(16) Ren, L.; Grina, J.; Moreno, D.; Blake, J. F.; Gaudino, J. J.; Garrey, R.; Metcalf, A. T.; Burkard, M.; Martinson, M.; Rasor, K.; Chen, H.; Dean, B.; Gould, S. E.; Pacheco, P.; Shahidi-Latham, S.; Yin, J.; West, K.; Wang, W.; Moffat, J. G.; Schwarz, J. B. *J. Med. Chem.* **2015**, *58*, 1976.

(17) Blake, J. F.; Chicarelli, M. J.; Garrey, R. F.; Gaudino, J.; Grina, J.; Moreno, D. A.; Mohr, P. J.; Ren, L.; Schwarz, J.; Chen, H.; Robarge, K.; Zhou, A., **2013**, WO2013130976A1.

(18) Compound **5** was prepared from commercially-available 4-chloro-2-(methylthio)pyrimidine and 2-fluoro-4-iodopyridine via a 2-step sequence.

(19) For recent reviews on asymmetric reduction of ketones using biocatalysis, see: (a) Matsuda, A.; Yamanaka, R.; Nakamura, K. *Tetrahedron: Asymmetry* **2009**, *20*, 513. (b) Moore, J. C.; Pollard, D. J.; Kosjek, B.; Devine, P. N. *Acc. Chem. Res.* **2007**, *40*, 1412. (c) Nakamura, K.; Yamanaka, R.; Matsuda, T.; Harada, T. *Tetrahedron: Asymmetry* **2003**, *14*, 2659.

(20) Compound **11** was prepared from commercially-available chloroacetyl chloride and 4-bromo-1-chloro-2-fluorobenzene via a 3-step sequence.

(21) Ruthenium-catalyzed asymmetric ketone reduction was initially attempted. Modest enantioselectivities were obtained via an asymmetric transfer hydrogenation reaction using Noyori´s protocol. For review on ruthenium-catalyzed asymmetric transfer hydrogenation: Noyori, R.; Hashiguchi, S. *Acc. Chem. Res.* **1997**, *30*, 97.

(22) Bachmann, S.; Fettes, A.; Iding, H.; Wirz, B.; Zutter, U., **2011**, WO2011023706A1.

(23) Several leaving groups including methanesulfonate, toluenesulfonate, chloromethanesulfonate and trifluoromethanesulfonate were studied, and the methanesulfonate group showed superiority over other derivatives. Preparation of toluenesulfonate required much longer time and the S_N2 reaction profile was similar to methanesulfonate. Chloromethanesulfonate and trifluoromethanesulfonate both showed some decomposition during the preparation.

(24) Both pyrimidine *N*-oxide impurities were observed after the oxidation reaction. The regioisomer of **13** was purged below the detection limit in the downstream process. Only the *N*-oxide derived from **13** was detected in the final API. In-silico GTI assessment was performed and indicated no structural alerts for either pyrimidine *N*-oxides of API.

(25) Noyori, R.; Aoki, M.; Sato, K. *Chemical Communications* **2003**, 1977.

(26) Cohen, D.; Cosbie, A.; Milburn, R. R.; Shaw, S.; Xie, Y. *Org. Proc. Res. Dev.* **2014**, *18*, 1807.

(27) Hirt, H.; Haenggi, R.; Reyes, J.; Seeger-Weibel, M.; Gallou, F. *Org. Proc. Res. Dev.* **2008**, *12*, 111.

(28) Waser, M.; Moher, E. D.; Borders, S. S. K.; Hansen, M. M.; Hoard, D. W.; Laurila, M. E.; LeTourneau, M. E.; Miller, R. D.; Phillips, M. L.; Sullivan, K. A.; Ward, J.

A.; Xie, C.; Bye, C. A.; Leitner, T.; Herzog-Krimbacher, B.; Kordian, M.; Müllner, M. *Org. Proc. Res. Dev.* **2011**, *15*, 1266.

(29) Kirk-Othmer Encyclopedia of Chemical Technology. 4th ed. Volumes 1: New York, NY. John Wiley and Sons, 1991-Present., p. V13 (95) 962.

(30) Shilcrat, S. *Org. Proc. Res. Dev.* **2011**, *15*, 1464.

(31) Hida, T.; Fukui, Y.; Kawata, K.; Kabaki, M.; Masui, T.; Fumoto, M.; Nogusa, H. *Org. Proc. Res. Dev.* **2010**, *14*, 289.

(32) High water content can also significantly minimize formation of the genotoxic impurity methyl benzenesulfonate during the salt formation. For more information, see: Teasdale, A.; Delaney, E. J.; Eyley, S. C.; Jacq, K.; Taylor-Worth, K.; Lipczynski, A.; Hoffmann, W.; Reif, V.; Elder, D. P.; Facchine, K. L.; Golec, S.; Schulte Oestrich, R.; Sandra, P.; David, F. *Org. Proc. Res. Dev.* **2010**, *14*, 999.